DOI: 10.24352/UB.OVGU-2017-064 TECHNISCHE MECHANIK, 34, 3-4, (2014), 222 – 232
submitted: October 16, 2013

Atomistic Simulation of Crystal Change and Carbon Diffusion during Drawing of Pearlitic Steel Nano-sized Wire

K. Saitoh, Y. Sameshima, M. Takuma, Y. Takahashi

Wire drawing is an efficient material processing technique for metals. Pearlitic steel is recognized as one of the most reliable and strong wire materials for industrial use. The microstructure of the pearlite phase, however, is quite complicated, with a lamellar structure containing alternating nanometer-thick layers of ferrite and cementite. In the present study, three-dimensional wire drawing models for pearlitic steel, in which a cementite layer occupies one half or one third of the wire cross section, are used in molecular dynamics simulations of the Fe-C system based on a pairwise potential. The results indicate that a body-centered cubic to face-centered cubic phase transition occurs in the ferrite layer during drawing. It is found that compressive hydrostatic stress is required to drive this phase transformation. The phase transition is followed by the formation of dislocations and grain boundaries. Cementite has an orthorhombic crystal structure and is more difficult to plastically deform than pure ferrite. During drawing of a pearlite wire, the large deformation of the ferrite layer compensates for the poor deformability of the cementite layer. The carbon content is important in pearlitic steel because carbon atoms can diffuse through all phases. As a indicator of the amount of carbon diffusion, the mean square displacement of carbon atoms is used. It is found that diffusion perpendicular to the ferrite/cementite interface tends to take place suddenly, but the total amount of diffusion is still less than that in the parallel direction.

1 Introduction

Wire drawing is an effective plastic working process for manufacturing wire or rod shapes. In this process, metals can be molded to a prescribed diameter (Sachs, 1954). For iron and steel materials, a group of pearlitic steels is well used in wiredrawing process. A pearlite microstructure is hoped to provide wires with excellent strength and ductility. However, steel is essentially a compound containing iron and carbon atoms. At the microstructure level, pearlitic steel is a kind of composite material comprising different phases, and the complicated microstructural changes it undergoes are still not fully understood. Although wire drawing has typically been used to produce wires with diameters from mm to μm, there is recently a growing demand for much narrower wires. A method of producing wires with nanometer diameters does not yet exist, and it would be of considerable interest to determine whether it is theoretically possible. Therefore, in the present study, atomistic-level molecular dynamics (MD) simulations are carried out to determine the behavior of pearlitic steel on a nanometer scale during the wire drawing process. Although there have been many MD studies on nano-sized materials with a wire geometry (Park, 2006; Saitoh and Liu, 2009; Kang and Cai, 2010; Lao et al., 2013), none have considered wire drawing using a hollow die. Therefore, the present paper is the first report of a three-dimensional MD calculation model for wire drawing.

In the present study, pearlitic steel is modeled as a lamellar structure of ferrite (α-Fe) and cementite (iron carbide, Fe_3C) layers with nanometer thicknesses. Computations were first carried out to investigate the mechanical properties of a perfect cementite crystal, because there have been few MD analyses of cementite. Lamellar models for wire drawing were then constructed. Since the atomistic behavior of the interface between ferrite and cementite is of practical importance when manufacturing pearlitic steels (Takahashi et al., 2012), the present study also focuses on the effect of the interface on carbon diffusion. This paper first describes the wire drawing model used for pearlitic steel, including the justification for the potential function used, and the method chosen to model the cementite crystal structure. The calculation model for the wiredrawing process is then introduced and the calculation results are presented. The results are then discussed and the conclusions of this study are presented. Results of this study will benefit the future construction of nano-sized wiredrawing techniques and will give some insight into nano-scale material behavior of carbon steel used in today's wiredrawing industry.

2 Theory and Method

2.1 Potential Function for Carbon-iron System

In order to conduct MD simulations, a potential function is needed (Allen and Tildesley, 1987). In the present study on pearlitic steel, both carbon (C) and iron (Fe) atoms are modeled. To the authors' knowledge, there is no reliable and precise potential function for the Fe-C system. However, a simple Fe-C potential function has been proposed by Levchenko et al. (2009), based on the well-known Johnson pairwise potential (Johnson, 1964; Johnson et al., 1964). In the present study, this potential function is used to model the cementite crystal. The potential is defined in terms of three different interactions involving Fe and C atoms,

$$\phi_{Fe-Fe} = a_1(r - r_1)^3 + a_2 r - a_3 \tag{1}$$

$$\phi_{Fe-C} = -\varepsilon \left[2\left(\frac{r - r_c}{r_c - r_0}\right)^3 + 3\left(\frac{r - r_c}{r_c - r_0}\right)^2 \right] \tag{2}$$

$$\phi_{C-C} = A \exp\left(-\frac{r}{r_s}\right) \tag{3}$$

where a_1, a_2, a_3, r_1 are potential parameters which depend on the interatomic distance r, and r_0, r_c, ε and A are constants. The function for the C-C pair has a difficulty in that it produces only a repulsive force, which differs from actual C-C interactions. However, during the modeling process, the C atoms in both the cementite and ferrite phases are well dispersed, so that interactions between them can be considered to be rare. This potential model is used for the Fe-Fe interaction in ferrite as well as the ferrite Fe - cementite Fe interaction. The mechanical properties of cementite were first simulated to determine whether the above potential is appropriate for modeling pearlite. Thus, these functions are judged to be reasonable for simulating the pearlite phase.

2.2 Mechanical Properties of Cementite

As shown in Figure 1, the cementite unit cell contains three Fe atoms and one C atom, and the crystal structure is orthorhombic. The lattice constants are a_0=0.4253 nm, b_0=0.5089 nm, c_0=0.6743 nm and the angles are $\alpha_0 = \beta_0 = \gamma_0 = 90$, as determined experimentally (Wykoff, 1964). In order to simulate tensile loading of cementite, this unit cell is used as a building block to construct three large parallelepiped computational blocks (specimens). These are shown in Figure 2, where the longitudinal direction corresponds to the tensile direction. For the two or three atomic layers at both ends in the tensile direction, the atomic velocity is constrained to generate tensile strain. In the other two directions, the surfaces are free so that contraction is possible under tensile loading. In the constrained regions, the velocity is fixed at 5 m/s, which corresponds to a tensile strain rate ranging between 8.3×10^8 1/s and 13.0×10^8 1/s. These strain rates are absolutely higher than those in existing experimental setting value. However, since these specimens are much smaller than realistic specimens and contain no defects, it is acceptable to study the ideal deformation behavior of crystals even with somewhat artificial settings. In the simulations, the system temperature is fixed at 300 K.

Stress-strain curves for the three cementite models are shown in Figure 3. The results are compared with those for pure ferrite, for which the tensile direction is [001]. Here, we evaluate a gradient of the stress-strain curve which is calculated by using a straight line drawn between the origin and the apparent yield point (where the graph is showing a sudden drop of stress). Both the gradient of these stress-strain curves and the tensile strength (maximum stress) are larger for cementite than for ferrite. For cementite, the gradient is estimated to be 158.4, 177.4 and 162.7 GPa for the [100], [010] and [001] directions, respectively, whereas for ferrite, it is 120.4 for the [001] direction. The values for cementite are consistent with experimentally determined values of Young's moduli (Mizubayashi et al., 1999). But for ferrite, the curve shows a completely nonlinear behavior due to softning, and the gradient value is less than the experimental value of Young's modulus which is about 200 GPa. On the other hand, cementite behaves in a rigid and brittle manner. So, for cementite specimens, the gradients of stress-strain curves can be compared with the experimental Young's moduli. Moreover, the simulation results show that for cementite, the gradient and tensile strength are anisotropic, such that $[010] > [001] > [100]$.

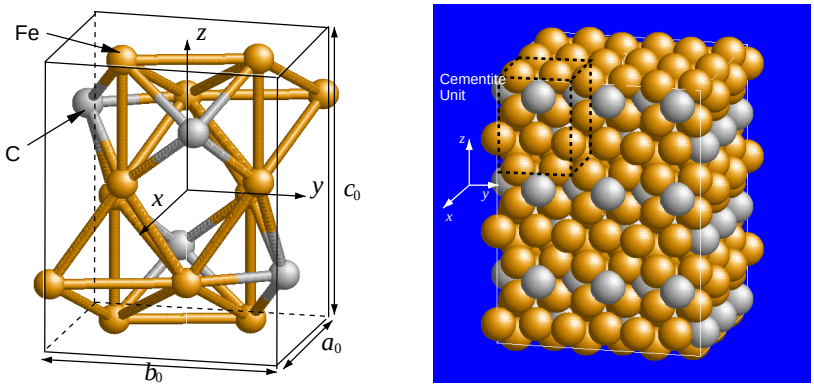

(a) crystal unit cell (b) cementite block ($3 \times 3 \times 3$ unit cells)

Figure 1: Orthorhombic unit cell of cementite and a constructed block

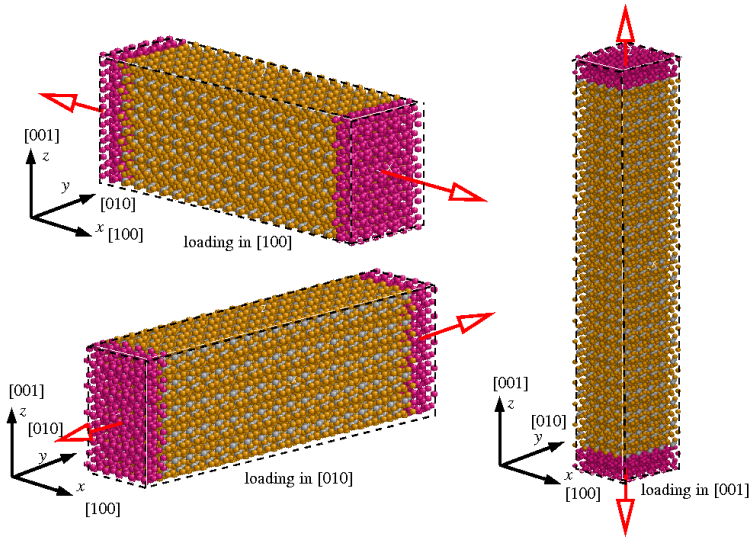

Figure 2: MD computational models of cementite specimens for tensile loading

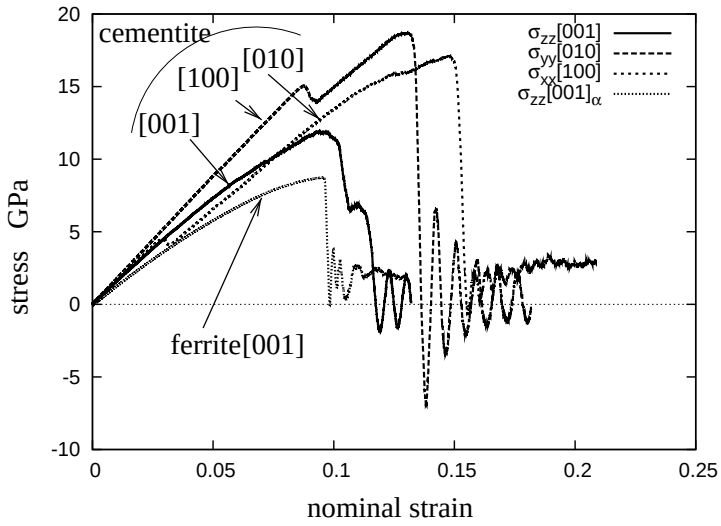

Figure 3: Stress-strain curves obtained by tensile simulation for cementite and ferrite specimens

2.3 Nano-sized MD Wire Drawing Model

For the MD simulations, two different pearlite models are constructed. The first is a two-layer model, in which a cementite layer and a ferrite layer are in direct contact with each other. The second is a three-layer model, in which a single cementite layer is sandwiched between two ferrite layers. Each layer forms a relatively thick plate, and the stacking direction is parallel to the wire axis. Although there have been some theoretical proposals for the structure of the cementite/ferrite interface, the following simplified structure is employed in the present study. A ferrite layer is placed so that its interface with the cementite layer is a $\{100\}$ plane in the body-centered cubic (bcc) crystal structure, and this interface is parallel to the drawing direction as shown in Figure 4. In both models, the layers are initially separated by a distance corresponding to half of the lattice constant for ferrite. Since this gives rise to an unstable interlayer, the models must be thermally stabilized. To achieve this, MD calculations are performed for 4 ps at a temperature of 10 K to allow structural relaxation.

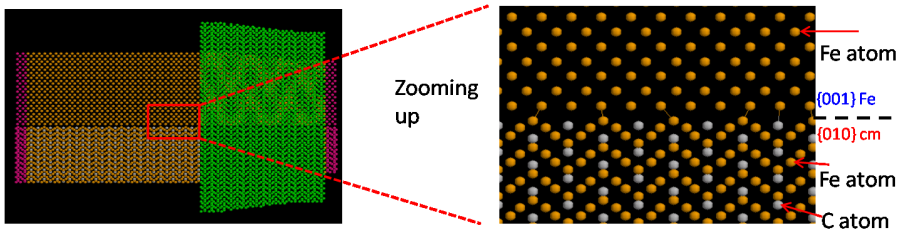

(a) before structural relaxation

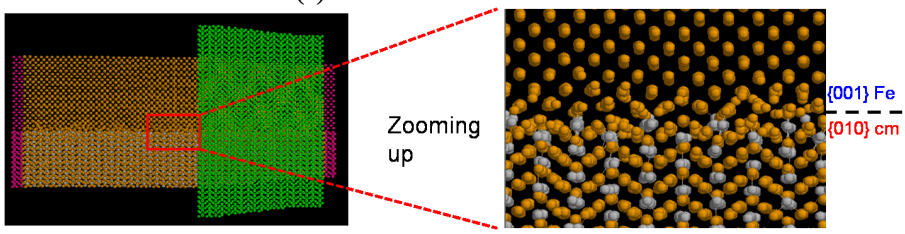

(b) after structural relaxation

Figure 4: Producing a stable interface between cementite and ferrite for the two-layer model of pearlitic steel

Figure 5 shows the two-layer and three-layer models used to simulate the wire drawing process for pearlitic steel. The wire has a cylinder shape to fit into the hole in the die, and is chucked at both ends. A constant velocity of 50 m/s is applied to the leading end, and the velocity of the other end is adjusted to be smaller in order to compensate for the reduction in area due to the die. The atoms in the die are completely constrained in three-dimensional space. In order to make the discussion clear, we omit the second one, three-layer model, in the result and discussion section later. And we would like to discuss the comparison as for the number of lamellae layers, elsewhere.

One crucial point to construct a better MD wiredrawing model is that one applies an adequate boundary condition. As a result, by adjusting the velocity of the end of the wire material, wiredrawing can proceed smoothly. It is also important to consider the friction between the die and the wire. On the nanometer scale, this is relatively straightforward since it can be assumed that friction is due to interatomic interactions between the die atoms and wire atoms. This means that most of the atoms around the die/wire interface interact with each other, giving rise to a large amount of friction that can cause the wire to stick. The solution of this is to reduce the amount of friction by modifying the strength of the interatomic interaction. This is a reasonable approach because, in actual wire drawing, a lubricant would be used. To mimic the lubricant without inserting a third element between the wire and the die, the potential function describing the interaction between the die and wire atoms is multiplied by a factor ω (< 1). Details of this method have been previously described and are omitted here (Saitoh et al., 2012). Previous simulations have shown that $\omega = 0.1$ or less leads to good lubrication and so this value is also used here. Since, in the present mode, the atoms inside the die are completely fixed at the same position as the initial one, their crystalline structure will little affect the dynamics of the wire atoms. Therefore, we set the crystalline structure of the die to the same as that of corresponding part of the wire. By doing so, we can exclude the complexity which will be caused by the difference between the crystal structures. In this method, no equilibrium bond length nor sliding strength is explicitly prescribed, but, thanks to reduction of the interaction, it becomes certainly easier for the wire atoms to slide along the die surface.

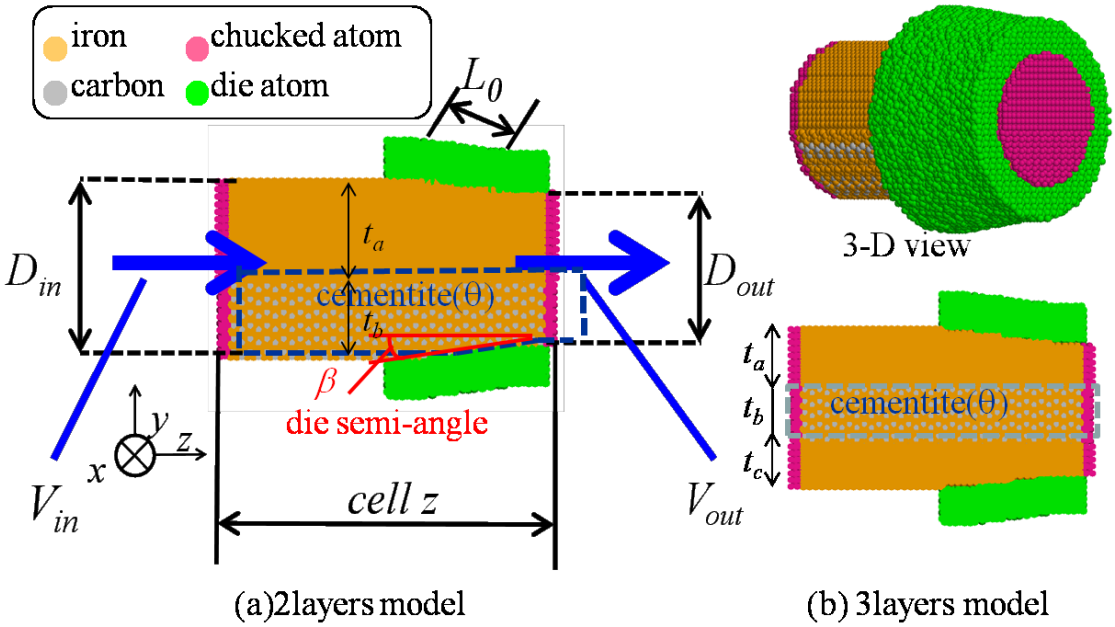

Figure 5: Two MD wire drawing models for pearlitic steel (For the interpretation with the reference to the colors in this figure, see the colored version of this article. (The three-layer model is not presented nor discussed in the present paper. It is shown just for reference.)

The calculation conditions are summarized in Table 1. The temperature is maintained at 10 K by the velocity scaling method. This prevents undesired heating of the wire which leads to atomic vibrations. Of course, the dependence on temperature is important, and this will be a subject for future study.

Table 1: Calculation conditions (The three-layer model is not presented nor discussed in the present paper. It is shown just for reference.)

Property	Units	two-layer model		three-layer model	
Ferrite layer thickness t_a, t_c	nm	3.73		2.29, 1.96	
Cementite layer thickness t_b	nm	3.01		2.35	
Die semi-angle β	°	7.0	10.0	7.0	10.0
Area reduction	%	27.1	37.3	27.1	37.3
Velocity V_{in}, V_{out}	m/s	36.4, 50.0	31.3, 50.0	36.4, 50.0	31.3, 50.0
Temperature	K	10.0			
Time increment of numerical integration	fs	2.0			
Friction factor ω	—	0.01 (only between die and wire atoms)			
Total number of atoms	—	78156	75690	78118	75715
Number of Fe atoms in ferrite layer	—	28990	28252	24782	23851
Number of Fe atoms in cementite layer	—	18253	17710	21364	21006
Number of C atoms in cementite layer	—	6086	5907	7145	7037
Number of atoms in die	—	24827	23821	24827	23821
Carbon content	wt.%	2.69	2.68	3.22	3.26

2.4 Analysis of Crystal Environment

In the MD simulations, not only the atomic configuration but also the crystalline environment can be determined. This is achieved by applying a common neighbor analysis (CNA) (Honeycutt and Andersen, 1987) to the simulation results. Using a CNA, the local environment can be categorized into bcc, face-centered cubic (fcc), hexagonal close packed (hcp), under-coordinated (defect or boundary), or over-coordinated (defect or boundary). The coordination number N_c for bcc (up to second-nearest neighbors) is 14. For fcc and hcp, N_c has a value of 12 considering just nearest neighbors. Such atoms are considered to be in a perfectly crystalline environment. However, atoms with other N_c values exist at defects or surfaces. Theory and detail of the CNA analysis can be found in Honeycutt

and Andersen (1987) and Tsuzuki et al. (2007). In the present study, the CNA category for each atom is indicated by the colors listed in Table 2 (For the interpretation with the reference to the colors, see the colored version of this article).

Table 2: CNA categories and visualization colors (For the interpretation with the reference to the colors in this figure, see the colored version of this article.)

Crystalline environment	Coordination number (N_c)	Color
bcc	14 (up to 2nd neighbors)	yellow
fcc	12 (up to 1st neighbors)	light gray
hcp	12 (up to 1st neighbors)	magenta
surface, defect or boundary	< 12	blue
defect or boundary	13 or > 14	brown

3 Results and Discussion

3.1 Phase Transition in Ferrite

Figure 6 shows the time evolution of the atomic configuration during a wire drawing simulation for the two-layer model with a die semi-angle of $\beta = 7.0°$. The time indicated is the total time elapsed since the beginning of the wire drawing process. The view is a cross section through the center of the wire and the die. The atoms are colored based on the results of a CNA analysis.

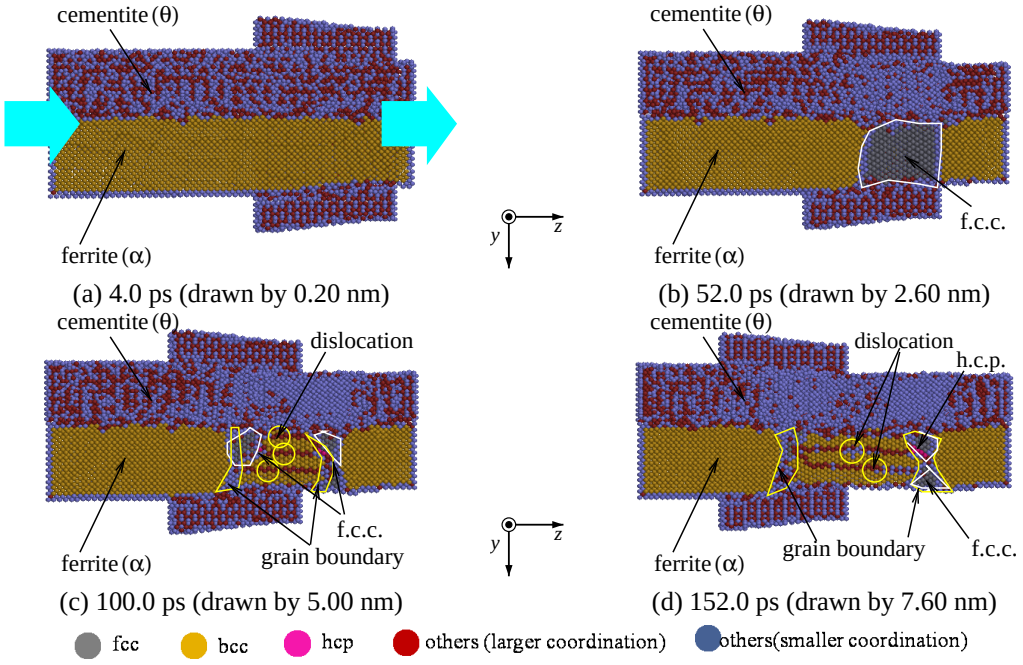

Figure 6: Atomic configuration for pearlite two-layer model ($\beta = 7.0°$) following CNA analysis. Different phases and defects are indicated by arrows. (For the interpretation with the reference to the colors in this figure, see the colored version of this article.)

It can be clearly seen that part of the originally bcc ferrite layer transforms into an fcc phase during the drawing process. Figure 7 shows a comparison between the results obtained for die semi-angles of $\beta = 7.0°$ and $\beta = 10.0°$. A larger angle leads to more deformation and a higher deformation rate. It can be seen that for the higher deformation rate (Figure 7(b-1),(b-2)), $\beta = 10.0°$), a larger fcc region is generated. When the fcc phase is subjected to further loading, stacking faults are sometimes introduced, which can cause the region to be again identified as hcp. These results indicate that the plastic deformation during wire drawing is capable of causing nanometer-scale phase transformations. This seems surprising since no such behavior has been ever been observed during drawing of a steel wire. However, the results of the present study suggest that it is in fact possible, and this may be supported by experimental observations of severe plastic deformation in steel materials produced by e.g., shot-pinning (Li

et al., 2008; Umemoto et al., 2008). At present, any exact nucleation site (atom) of bcc-to-fcc transition has not yet been detected or determined with fine resolution. We believe this is worthwhile studying and will be studied further in the future.

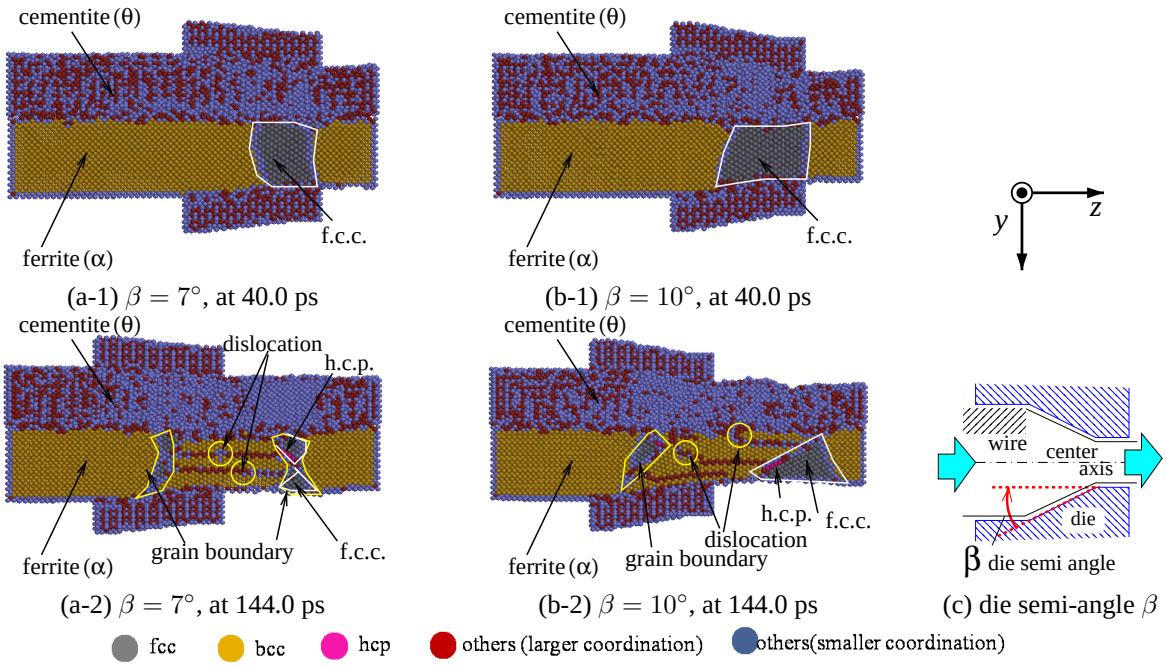

Figure 7: Transition to fcc phase in ferrite for different die semi-angles β. Different phases and defects are indicated by arrows. (For the interpretation with the reference to the colors in this figure, see the colored version of this article.)

When the ferrite layer is observed in more detail, the appearance of both dislocations and grain boundaries is apparent, as shown in Figure 8. Dislocations begin from where crystal slip planes are terminated by grain boundaries. It is interesting that when the die semi-angle β is large, the ferrite/cementite interface also becomes other emission sites (shown in Figure 8(b)).

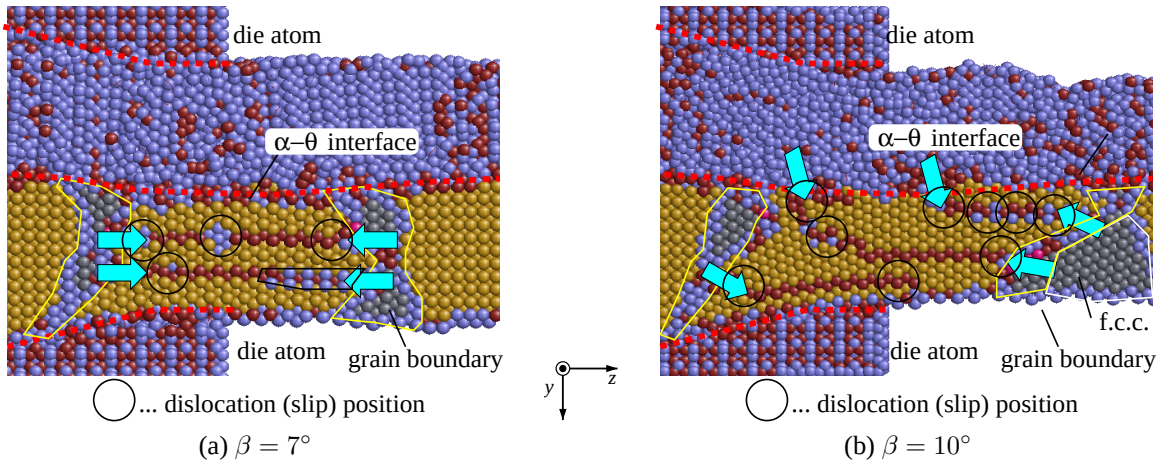

Figure 8: Formation of dislocations and grain boundaries during wire drawing (arrows indicate observed dislocation nucleation sites).

3.2 Wire Stress During Drawing Process

The stress field that is present during the wire drawing process has been extensively studied using continuum analysis approaches such as finite element method simulations (McAllen and Phelan, 2007), and it is known to be unique. It is therefore of interest to investigate the stress distribution while drawing wires with nanometer

dimensions, particularly since Figure 7 indicates that the extent of the phase transition depends principally on the amount of stress. Here, the generic hydrostatic stress σ_m and equivalent (von Mises) stress σ_{eq} are considered. Figure 9 shows the time evolution of the average σ_m value in the ferrite and cementite regions during the drawing process for different die semi-angles. For the cementite layer, σ_m can be positive or negative. However, for the ferrite layer, it is always negative (compressive), including during the bcc-to-fcc phase transition. This indicates that the phase transition requires a large negative triaxial stress, i.e., a compressive hydrostatic stress component. This is consistent with the results of steel shot-peening experiments, where a phase transition occurs under the influence of a large compressive hydrostatic component. Though, the hydrostatic stress required for bcc-to-fcc transformation has not been reported based on the experiment. It is supposed that it is of an order comparable with the Vickers hardness of transformed surface in the specimen, which is above 6 GPa. It is likely that our simulation results show a smaller value than that of the experiment.

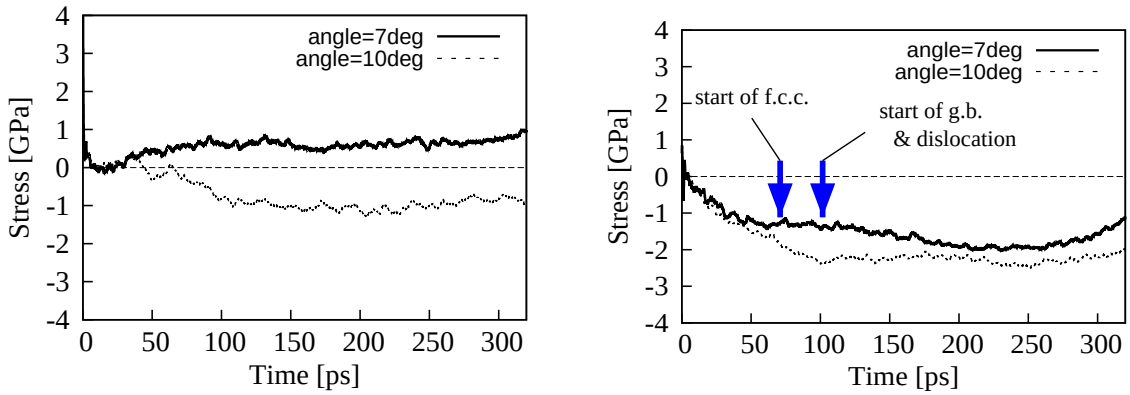

(a) cementite phase (b) ferrite phase

Figure 9: Average hydrostatic stress in the cementite and ferrite phases of a pearlite wire (two-layer model)

Figure 10 shows the average equivalent stress σ_{eq} in the combined cementite and ferrite phases and in the ferrite phase only. It is known that at a certain value of σ_{eq} plastic flow occurs in a material. For the combined cementite and ferrite phases, σ_{eq} soon saturates as it becomes flow stress. However, for the ferrite region, it continues to decrease with time. Thus, when a pearlite wire is subjected to plastic loading, the ferrite phase is the first to deform, and it undergoes more deformation than cementite. In other words, it is difficult for the cementite θ phase to plastically deform (Saitoh et al., 2012), but the ferrite undergoes easy deformation. Consequently, the softness and ductility of the ferrite phase compensates for the hardness and brittleness of the cementite phase. This easy deformability of the ferrite phase is clear from the results shown in Figure 3.

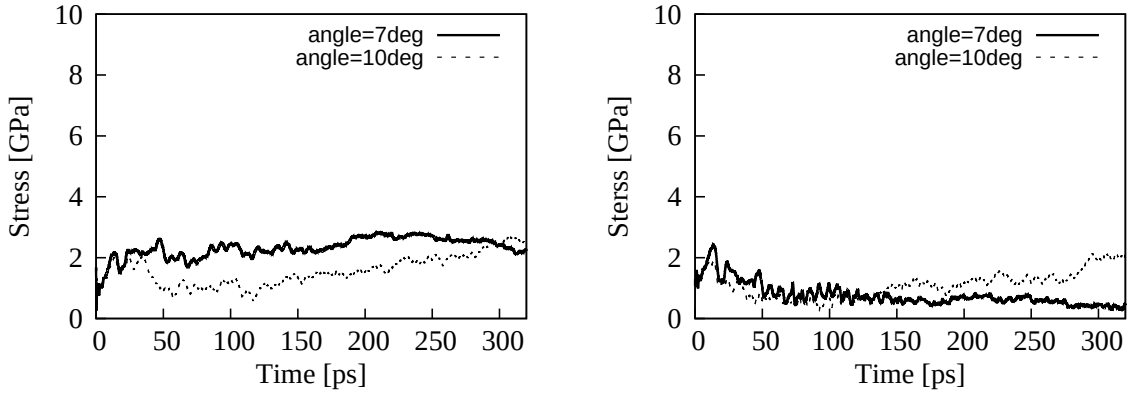

(a) combined cementite and ferrite phases (b) ferrite phase only

Figure 10: Average equivalent stress (von Mises) in pearlite wire (two-layer model)

3.3 Atomic Diffusion in the Vicinity of the Cementite/Ferrite Interface

The diffusion mechanism for carbon atoms during the wire drawing process has also been investigated. Carbon atoms initially contained in the cementite phase may move into the ferrite phase and occupy interstitial positions for some time. An experimental study on heavily drawn pearlitic steel has shown that disordering or melting of the cementite phase takes place and C atoms diffuse across the interface into the ferrite phase (Li et al., 2012). Figure 11 shows the mean squared displacement (MSD) of C atoms around the cementite/ferrite interface for the two-layer pearlite model. The slope of the MSD increases both with the amount of deformation (die semi-angle) and the temperature. Figures 11(a) and 11(b) show the MSD in the directions parallel and perpendicular to the interface, respectively, and they are quite different. Generally speaking, diffusion occurs more readily in the direction parallel to the interface, and it is difficult for C atoms to enter the ferrite layer because C has a low solubility limit in the bcc structure. But, as found in Figure 11(a), MSD of C atoms drastically increases just when the cementite/ferrite interface begins to pass through the die. It may be concluded that carbon diffusion is enhanced by the wire drawing process.

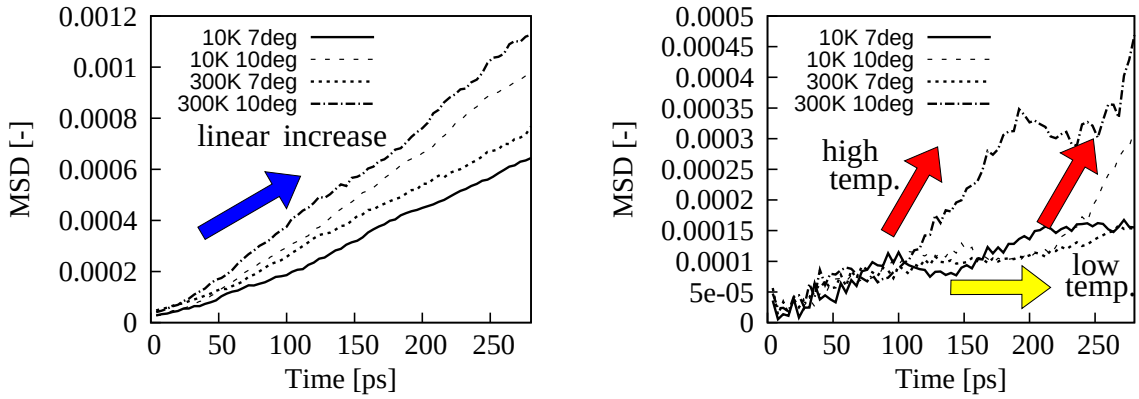

(a) Parallel to interface

(b) Perpendicular to interface

Figure 11: MSD of carbon atoms during wire drawing process

3.4 Discussion

The relationship among the stress state, phase transition and carbon diffusion during the wire drawing process is schematically illustrated in Figure 12. The following sequence of events is thought to occur:

- When the wire is drawn, the hydrostatic stress increases in the ferrite layer.
- Some regions of the bcc ferrite layer transform into the fcc phase.
- Carbon atoms, which have been melted from the cementite layer, move to the cementite/ferrite interface. These atoms diffuse along the interface and some of them cross it.
- The fcc phase disappears, but grain boundaries and defects remain inside the wire.

4 Conclusions

Three-dimensional molecular dynamics modeling of the wire drawing process for pearlitic steel, containing cementite and ferrite phases, is carried out. Careful consideration is given to simulation parameters such as the potential function, crystalline orientation and die geometry, in order to accurately reproduce the actual material behavior. The following results are obtained:

1. For a cementite crystal, a large anisotropy is found for the gradient of the increasing part in stress-strain curve (which reflects the value of Young's modulus) and tensile strength.

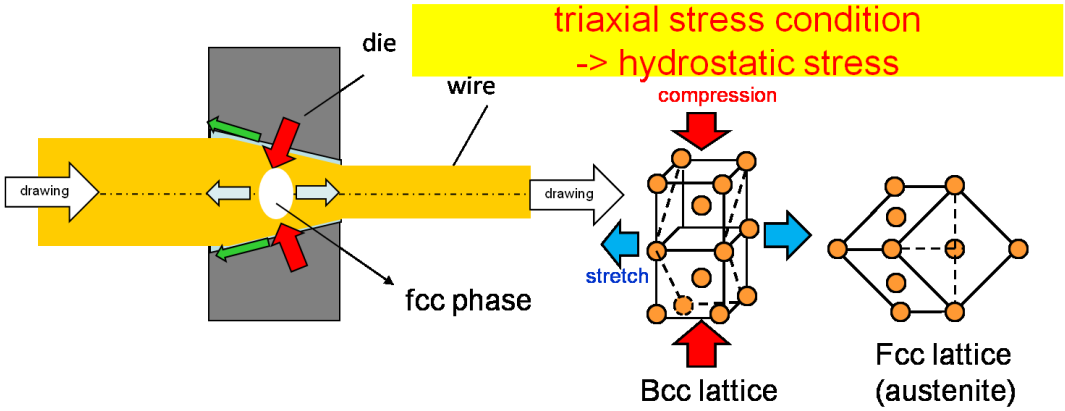

Figure 12: Relationship among stress state, phase transition and carbon diffusion during drawing process

2. During the drawing process, a bcc-to-fcc phase transition occurs in the ferrite layer, in addition to plastic deformation associated with dislocation motion. The main reason for this phase change is thought to be an increase in the hydrostatic stress in the wire inside the die.

3. Carbon diffusion is found to occur in the vicinity of the cementite/ferrite interface, and becomes more significant with increasing plastic deformation and temperature. However, only a limited amount of diffusion occurs into the ferrite layer.

Acknowledgements

This study was supported in part by the ”Strategic Project to Support the Formation of Research Bases at Private Universities: Matching Fund Subsidy from MEXT (Ministry of Education, Culture, Sports, Science and Technology) (2012-2013).” The authors also acknowledge Nippon Steel & Sumitomo Metal Co., Ltd., and Kurimoto Ltd. for financial support.

References

Allen, M.; Tildesley, D.: *Computer simulation of liquids*. Oxford University Press (1987).

Honeycutt, J.; Andersen, H.: Molecular dynamics study of melting and freezing of small lennard-jones clusters. *J.Phys.Chem.*, 19, (1987), 4950 – 4963.

Johnson, R.: Interstitials and vacancies in α iron. *Phys.Rev.,A*, 134, (1964), A1329 – A1336.

Johnson, R.; Dienes, G.; Damask, A.: Calculations of the energy and migration characteristics of carbon and nitrogen in α-iron and vanadium. *Acta Metall.*, 12, (1964), 1215 – 1224.

Kang, K.; Cai, W.: Size and temperature effects on the fracture mechanisms of silicon nanowires: molecular dynamics simulations. *Int.J.Plast.*, 26, (2010), 1387 – 1401.

Lao, J.; Tam, M.; Pinisetty, D.; Gupta, N.: Molecular dynamics simulation of fcc metallic nanowires: a review. *JOM*, 65, 2, (2013), 175 – 184.

Levchenko, E.; Evteev, A.; Belova, I.; Murch, G.: Molecular dynamics simulation and theoretical analysis of carbon diffusion in cementite. *Acta Mater.*, 57, (2009), 846 – 857.

Li, J.; Umemoto, M.; Todaka, Y.; Fujisaku, K.; Tsuchiya, K.: The dynamic phase transformation and formation of nanocrystalline structure in sus304 austenitic stainless steel subjected to high pressure torsion. *Rev.Adv.Mater.Sci.*, 18, (2008), 577 – 582.

Li, Y.; Choi, P.; Goto, S.; Borchers, C.; Raabe, D.; Kirchheim, R.: Evolution of strength and microstructure during annealing of heavily cold-drawn 6.3 gpa hypereutectoid pearlitic steel wire. *Acta Mater.*, 60, (2012), 4005 – 4016.

McAllen, P.; Phelan, P.: Numerical analysis of axisymmetric wire drawing by means of a coupled damage model. *J.Mater.Process.Technol.*, 183, (2007), 210 – 218.

Mizubayashi, H.; Li, S.; Yumoto, H.; Shimotomai, M.: Young's modulus of single phase cementite. *Scripta Mater.*, 40, 7, (1999), 773 – 777.

Park, H.: Stress-induced martensitic phase transformation in intermetallic nickel aluminum nanowires. *Nano Lett.*, 6, 5, (2006), 958 – 962.

Sachs, G.: *Fundamentals of the working of metals*. Pergamon press, London (1954).

Saitoh, K.; Daira, S.; Sameshima, Y.: Nano-scale modelling and simulation of metal wiredrawing by using molecular dynamics method. *Proceedings of International Conference on Materials Processing and Technology 2012 (MAPT2012)*, 211 – 216.

Saitoh, K.; Liu, W.: Molecular dynamics study of surface effect on martensitic cubic-to-tetragonal transformation in Ni-Al alloy. *Comput.Mater.Sci.*, 46, 2, (2009), 531 – 544.

Takahashi, J.; Kosaka, M.; Kawakami, K.; Tarui, T.: Change in carbon state by low-temperature aging in heavily drawn pearlitic steel wires. *Acta Mater.*, 60, (2012), 387 – 395.

Tsuzuki, H.; Branicio, P.; Rino, J.: Structural characterization of deformed crystals by analysis of common atomic neighborhood. *Computer Phys.Commun.*, 177, (2007), 518 – 523.

Umemoto, M.; Todaka, Y.; Li, J.: Change in microstructure and mechanical properties of steel components surface layer by severe plastic deformation. *Tetsu-to-Hagane*, 94, 12, (2008), 616 – 628.

Wykoff, R.: *Crystal structures*. Interscience, New York (1964).

Address: Saitoh, Ken-ichi, Materials and Mechanics Laboratory, Department of Mechanical Engineering, Faculty of Engineering Science, Kansai University, Osaka, Japan
email: saitou@kansai-u.ac.jp